STEM CELLS AND DEVELOPMENT
Volume 22, Number 12, 2013

DOI: 10.1089/scd.2012.0653

MicroRNA-122 Influences the Development of Sperm Abnormalities from Human Induced Pluripotent Stem Cells by Regulating *TNP2* Expression

Te Liu,[1–3] Yongyi Huang,[4] Jianjun Liu,[5] Yanhui Zhao,[6] Lizhen Jiang,[4,7] Qin Huang,[4,7] Weiwei Cheng,[1] and Lihe Guo[4,7]

Sperm abnormalities are one of the main factors responsible for male infertility; however, their pathogenesis remains unclear. The role of microRNAs in the development of sperm abnormalities in infertile men has not yet been investigated. Here, we used human induced pluripotent stem cells to investigate the influence of miR-122 expression on the differentiation of these cells into spermatozoa-like cells in vitro. After induction, mutant miR-122-transfected cells formed spermatozoa-like cells. Flow cytometry of DNA content revealed a significant increase in the haploid cell population in spermatozoa-like cells derived from mutant miR-122-transfected cells as compared to those derived from miR-122-transfected cells. During induction, TNP2 and protamine mRNA and protein levels were significantly higher in mutant miR-122-transfected cells than in miR-122-transfected cells. High-throughput isobaric tags for relative and absolute quantification were used to identify and quantify the different protein expression levels in miR-122- and mutant miR-122-transfected cells. Among all the proteins analyzed, the expression of lipoproteins, for example, APOB and APOA1, showed the most significant difference between the two groups. This study illustrates that miR-122 expression is associated with abnormal sperm development. MiR-122 may influence spermatozoa-like cells by suppressing *TNP2* expression and inhibiting the expression of proteins associated with sperm development.

Introduction

Recent technological developments in in vitro fertilization have enabled the occurrence of pregnancy and live births despite low sperm activity [1]. The number of patients with infertility due to sperm abnormalities has been increasing every year, which is a cause for concern. Sperm abnormalities are a form of male infertility that present in a variety of ways, and may prevent the spermatozoa from achieving fertilization [2–5]. Previous studies have shown several causes of abnormal semen exist, including infection with sexually transmitted diseases, retrograde ejaculation, and inability of the semen to clot properly, all of which can significantly affect male fertility. In addition, spermatozoa abnormalities may be inherited or caused by hormone imbalance, medication, or recent infection [6]. Although previous experiments have implicated many genes in male sterility in mice, it is possible that mutations in these genes are also related to human infertility [1,7,8]. However, the detailed molecular mechanisms behind infertility remain uncertain. As reported previously, transition nuclear protein genes (*TNP*s) play an important role in nuclear formation during spermiogenesis [1,7–11].

Major chromatin restructuring occurs in elongating and condensing spermatids, which are in turn replaced by protamines (PRMs) [12–15]. TNPs are arginine- and lysine-rich basic proteins that strongly bind to DNA, and are expressed exclusively in postmeiotic haploid spermatids. In mice, *TNP2* mRNAs are first detected in step 7 round spermatids, and are then degraded at steps 13 and 14, respectively [12,14,15]. Furthermore, *TNP*s are phosphorylated by sperm-specific protein kinase A, and this phosphorylation/dephosphorylation cycle

[1]International Peace Maternity and Child Health Hospital, Shanghai Jiaotong University, Shanghai, China.
[2]School of Environmental Science and Engineering, Donghua University, Shanghai, China.
[3]Shanghai Geriatric Institute of Chinese Medicine, Longhua Hospital, Shanghai University of Traditional Chinese Medicine, Shanghai, China.
[4]Sino-America United Stem Cell Research Center, Shanghai, China.
[5]Shanghai Second People's Hospital, Shanghai, China.
[6]Shanghai Key Laboratory of Stomatology, Department of Oral & Cranio-Maxillofacial Science, Shanghai Ninth People's Hospital, Shanghai JiaoTong University School of Medicine, Shanghai, China.
[7]Institute of Biochemistry and Cell Biology, Shanghai Institute for Biological Sciences, Chinese Academy of Sciences, Shanghai, China.

has been found to play an important role in the chromatin condensation process [9–11]. *TNP*s are removed from condensing chromatin and replaced by PRMs [13], which constitute the major nuclear proteins of condensed spermatids and mature spermatozoa [12,14–16]. Miyagawa et al. demonstrated single-nucleotide polymorphisms (SNPs) and specific variability in the *TNP* genes of sterile male patients [1]. Moreover, Tseden et al. used transgenic mice to confirm that premature translation of *TNP2* mRNA could result in abnormal head morphogenesis, reduced sperm motility, and male infertility [7]. Furthermore, Shirley et al. suggested that each TNP fulfilled a unique function during spermiogenesis, even though the sperm phenotypes strongly indicated that the defects were largely attributable to an overall gene dosage effect [8]. They reported that *TNP* null mutant mice were subfertile, while mice lacking both *TNP* genes were infertile, indicating that the sperm of *TNP*-null double-mutant mice tended to have abnormalities and reduced reproductive capacity [8]. Therefore, these results clearly illustrate that strict temporal and stage-specific translation of *TNP* is necessary for the correct differentiation of round spermatids into mature spermatozoa and for male fertility.

Furthermore, other studies have demonstrated the importance of PRMs in the morphogenesis and function of mature spermatozoa [17,18]. PRMs are a diverse family of small arginine-rich proteins that have been found to be synthesized in the late-stage spermatids of many animals and plants. These PRMs bind to DNA, condensing the spermatid genome into a genetically inactive state [17]. They are characterized by a number of arginine residue stretches separated by neutral amino acids. Fiber-diffraction diagrams from reconstituted nucleoprotamine and whole sperm cells indicated that the DNA molecules were tightly packed in a hexagonal unit cell, and that DNA was in a B-like structure with 10 base pairs per helical turn [18]. PRM1 and PRM2, the two PRMs found in mammals, are the most widely studied. Sperm DNA is packaged by PRM1 in all mammals, whereas PRM2 is present only in the sperm of primates, several species of rodents, and a subset of other placental mammals. Both PRMs are phosphorylated soon after their synthesis; however, after binding to DNA, most phosphate groups are removed and cysteine residues are oxidized, forming disulfide bridges linking the PRMs [17]. PRM2 (but not PRM1) is synthesized as a precursor that undergoes proteolytic processing after binding to DNA. It also binds to a zinc atom, albeit its function is not yet known [17,18].

We previously determined the importance of TNPs and PRMs in sperm maturation [19]; however, very little is known about the mechanisms by which they are regulated during sperm development. MicroRNAs (miRNAs), a class of ~22-nucleotide (nt) noncoding RNAs, participate in diverse biological functions by promoting the degradation or inhibiting the translation of their target mRNAs [19–27]. Recent findings that individual miRNAs are expressed during spermatogenesis in a developmental stage-specific manner suggest that miRNAs participate in male germ cell development, by contributing to cell type-specific protein expression profiles during spermatogenesis [20]. Yu et al. first reported that miR-122 negatively regulates *Tnp2* mRNA by endonucleolytic cleavage, due to specific base pair interactions of miR-122 with its complementary binding sequence in the 3′-untranslated region (3′-UTR) of *Tnp2* mRNA [21]. Meanwhile, Dai et al. also revealed that expression of testis-specific miR-469 bound to the coding region and repressed the translation of *Tnp2* and *Prm2* mRNA, to regulate the development and maturation of sperm cells [20].

On the other hand, in a previous study, miRNA microarray analysis was used to identify the miRNAs that are differentially expressed in abnormal infertile semen and normal fertile semen [19]. Microarray analysis revealed significant overexpression of 21 miRNAs in abnormal semen, as compared to normal semen. Furthermore, 31 miRNAs were expressed at significantly lower levels in abnormal semen than in normal semen (Supplementary Table S1; Supplementary Data are available online at www.liebertpub.com/scd). We found that miR-122 expression was significantly different in healthy semen and infertile semen (Supplementary Fig. S1). Moreover, northern blotting and microRNA-specific quantitative real-time reverse transcription PCR (miR-qRT-PCR) revealed that the miR-122 hybridization signals were weaker in the semen from the healthy controls than in infertile semen, confirming that miR-122 was upregulated in the abnormal sperm. Thus, preliminary experiments revealed that miR-122 was closely associated with the occurrence of abnormal spermatozoa. Based on this evidence, we hypothesized that miR-122 may influence the formation of abnormal sperm by regulating of TNP2 protein expression. Therefore, we used human induced pluripotent stem (iPS) cells as an in vitro development model in this study. We used molecular biology and proteomics approaches to analyze miRNA-122 expression, to determine whether or not miRNA-122 influences sperm morphogenesis by regulating the expression of crucial proteins involved in sperm development during the differentiation of iPS cells into spermatozoa-like cells.

Materials and Methods

Human iPS cells cultured, embryoid bodies formation, and induced differentiation into spermatozoa-like cells

The human iPS cells were generated as previously described [27,28]. Briefly, iPS cultures were separated from the feeder cells by treatment of 0.125% trypsin–EDTA solution and plated onto and co-cultured with MEFs. The cells were cultured in DMEM:F12 (1:1) medium supplemented with 15% KnockOut™ Serum Replacement, 1 mM sodium pyruvate, 2 mM L-glutamine, 0.1 mM nonessential amino acids, 0.1 mM beta-mercaptoethanol, and penicillin (25 U/mL)–streptomycin (925 mg/mL), and mixed. Those cells incubated in a humidified tissue culture incubator containing 5% CO_2 at 37°C. All cells were cultured on the same feeder until passage 10th before making ulterior experiments.

All steps were followed as previously described [29–32]. Briefly, for the formation embryoid bodies (EBs), the iPS cells were dissociated with 0.125% trypsin–EDTA solution and suspended onto Petri dishes with full medium for 6 days. Then, to induce EB differentiation, day 6 EBs were cultured in induced cell-conditioned medium [DMEM: F12 (1:1) medium supplemented with 5% KnockOut™ Serum Replacement, 1 mM sodium pyruvate, 2 mM L-glutamine, 0.1 mM nonessential amino acids, penicillin (25 U/mL)–streptomycin (925 mg/mL), 5 mg/mL transferrin, 10 mg/mL insulin, 10 ng/mL human epidermal growth factor, 10 ng/mL human basic fibroblast growth factor, 100 nM of human

testosterone, 100 mIU human follicle-stimulating hormone, 330 nM retinoic acid, and 330 ng/mL retinal, and mixed] and incubated in a humidified tissue culture incubator containing 5% CO_2 at 37°C for 10 days until differentiation completely.

Recombinant lentivirus generation vector construction and cell transfection

All steps of recombinant lentivirus package were according to the previously described [21,24,26,27]. The Ltv-miR-122 and Ltv-miR-122-mut lentivirus were built by Genepharma Corporation, and the methods of lentivirus transfected were according to the company's instructions. In addition, the negative control Ltv-miR-122-mut was similarly built, except that 22 nucleotides in sequences corresponding to miR-122 see sequences were mutated (change TGGAGTGTGACAATGGTGTTTG to TtcgGaGTtACAATG GcGTaaG, mutations shown in lower case). Briefly, human iPS cells were co-transfected to use 4×10^7 PFU/mL Ltv-miR-122 or Ltv-miR-122-mut lentivirus, respectively, according to the manufacturer's protocol. The iPS cells were seeded in a six-well plate and cultured in DMEM:F12 (1:1) medium supplemented with 15% KnockOut™ Serum Replacement, 1 mM sodium pyruvate, 2 mM L-glutamine, 0.1 mM nonessential amino acids, 0.1 mM beta-mercaptoethanol, and penicillin (25 U/mL)–streptomycin (925 mg/mL), and mixed. These cells were incubated in a humidified tissue culture incubator containing 5% CO_2 at 37°C until 80% confluent.

Luciferase report assay

All steps of the luciferase report assay were in accordance to the previously described [24–27]. NIH-3T3 cells were seeded at 3×10^4/well in 48-well plates and co-transfected with 400 ng of Ltv-miR-122 or Ltv-miR-122-mut vectors, 20 ng of pGL3-TNP2-3UTR-WT or pGL3-TNP2-3UTR-Mut, and pGL-TK (Progema) using Lipofectamine 2000 Reagent according to the manufacturer's protocol. After 48 h transfection, luciferase activity was measured using the dual-luciferase reporter assay system (Progema).

RNA extraction and analysis by quantitative real-time PCR

Total RNA from each cell was isolated with Trizol Reagent (Invitrogen, Life Technologies Corporation), according to the manufacturer's protocol. Briefly, sperm samples or cells (3×10^8/mL) were collected and added 0.8 mL Trizol Reagent. After incubating the sample for 5 min, 0.2 mL of chloroform was added, and the tubes were vigorously shook and incubated for 2 min. The samples were centrifuged 12,000 rpm for 15 min at 4°C. Then, the aqueous phases were transferred to clean tubes, and 0.4 mL of Isopropanol was added, and mixed. After centrifuging again, the total RNA could be collected. The RNA samples were treated with DNase I (Sigma-Aldrich), quantified, and reverse-transcribed into cDNA with the ReverTra Ace-First Strand cDNA Synthesis Kit [Toyobo, Toyobo (Shanghai) Biotech Co., Ltd.]. Quantitative real-time PCR was conducted with a RealPlex4 real-time PCR detection system from Eppendorf, with SyBR Green RealTime PCR Master Mix [Toyobo, Toyobo (Shanghai) Biotech Co., Ltd.] as the detection dye. Quantitative real-time PCR amplification was performed over 40 cycles with denaturation at 95°C for 15 s and annealing at 58°C for 45 s. Target cDNA was quantified with the relative quantification method. A comparative threshold cycle (Ct) was used to determine gene expression relative to a control (calibrator), and steady-state mRNA levels are reported as an *n*-fold difference relative to the calibrator. For each sample, the maker gene Ct values were normalized with the formula $\Delta Ct = Ct\_genes - Ct\_18S\ RNA$. To determine relative expression levels, the following formula was used: $\Delta\Delta Ct = \Delta Ct\_all\_groups - \Delta Ct\_control\_group$. The values used to plot relative expressions of markers were calculated with the expression $2^{-\Delta\Delta Ct}$. The mRNA levels were calibrated on the basis of levels of 18S rRNA. The cDNA of each gene was amplified with primers as Table 1 descriptions.

Northern blotting analysis

All steps of northern blotting were according to the previously described [26,27,33]. For all groups, 20 μg of good quality total RNA was analyzed on a 7.5 M ureum and 12% PAA denaturing gel and transferred to a Hybond N^+ nylon membrane (Amersham). Membranes were crosslinked using UV light for 30 s at 1,200 mJ/cm^2. Hybridization was performed with the miR-122 antisense starfire probe, 5′- CAAACACCATTGTC

Table 1. The Sequences of Human Gene Quantitative Real-time PCR Primer

Gene product	*Forward (F) and reverse (R) primers (5′→3′)*	*Size (bp)*
SERPINA1	F: CCACTGCTTAAATACGGACGA R: ACGAGACAGAAGACGGCATT	101
PIGR	F: TAGAGAGGCAGGGGTTACCA R: ACCACTCAGGCCGACTTCT	110
LGALS3BP	F: GAGGAGGCTCCACACGG R: AGCAGCCACACCCAGAAG	97
VWF	F: TCGGACCCTTATGACTTTGC R: TTTCCCCAGAGGAGATGTTG	106
MMRN1	F: CGCACTTAAGAAACCAACGG R: GATGCCGACTACAGCTTGAAT	110
APOE	F: CCAATCACAGGCAGGAAGAT R: CTCCGGCTCTGTCTCCAC	105
C3	F: CCTGGACTGCTGCAACTACA R: CTCACTTCGGGAAACGATGT	127
GPLD1	F: CTTTCCAGTGGCCACGTACT R: CTTGGTGTAGGGTCACGGTC	115
APOB	F: CCTAAAAGCTGGGAAGCTGA R: CCTCCGTTTTGGTGGTAGAG	107
ITIH1	F: GGCAGCCCAAACTATCAAGA R: CGTAGGTCACCTTGAAGTGC	134
FN1	F: GCAGCCTGCATCTGAGTACA R: GGTGGAATAGAGCTCCCAGG	111
HBA1/2	F: GGACCCGGTCAACTTCAA R: CAGGAACTTGTCCAGGGAGG	109
ITIH2	F: CTGGCACAAGGATCTCAGGT R: TTGAAACAAATGTTCTTTTGGC	106
IGFALS	F: ACAGCAGACGTACCCTCCC R: CAGTGCCACCCAGGACA	113
APOA1	F: TGGATGTGCTCAAAGACAGC R: TTGCTGAAGGTGGAGGTCAC	121
HBB	F: AGCTGCACTGTGACAAGCTG R: CACTGGTGGGGTGAATTCTT	110
18S rRNA	F: CAGCCACCCGAGATTGAGCA R: TAGTAGCGACGGGCGGTGTG	253

Table 2. Primary Antibodies List

Antibodies	*Companies*	*Applications*
Rabbit anti-human Oct4	Cell Signaling Technology	IF (1:200) WB (1:1,000)
Rabbit anti-human Nanog	Cell Signaling Technology	IF (1:200) WB (1:1,000)
Rabbit anti-human TNP2	Santa Cruz Technology	IF (1:200) WB (1:1,000)
Rabbit anti-human Protamine	Santa Cruz Technology	IF (1:200) WB (1:1,000)
Rabbit anti-human Histon 3	Cell Signaling Technology	IF (1:200) WB (1:1,000)
Rabbit anti-human β-actin	Cell Signaling Technology	WB (1:1,000)

IF, immunofluorescence staining; WB, western blotting analysis.

ACACTCCA-3′, to detect the 22-nt miR-122 fragments according to the instruction of the manufacturer. After washing, membranes were exposed for 20–40 h to Kodak XAR-5 films (Sigma-Aldrich).

Western blotting analysis

Cells were lysed using a 2× loading lysis buffer (50 mM Tris–HCl, pH 6.8, 2% sodium dodecyl sulfate, 10% β-mercaptoethanol, 10% glycerol, and 0.002% bromophenol blue). The total amount of proteins from the cultured cells was subjected to 12% SDS-PAGE and transferred onto Hybrid-PVDF membranes (Millipore). After blocking with 5% (w/v) nonfat dried milk in TBST (Tris-buffered saline containing Tween-20) (25 mM Tris/HCl, pH 8.0, 125 mM NaCl and 0.05% Tween-20), the PVDF membranes were washed 4 times (15 min each) with TBST at room temperature and incubated with primary antibody (Table 2). Following extensive washing, membranes were incubated with HRP-conjugated goat anti-rabbit IgG secondary antibody (1:1,000; Santa Cruz Technology) for 1 h. After washing 4 times (15 min each) with TBST at room temperature, the immunoreactivity was visualized by enhanced chemiluminescence using ECL kit from Perkin-Elmer Life Science.

Immunofluorescence staining

The cultured cells were washed 3 times with PBS and fixed with 4% paraformaldehyde (Sigma-Aldrich) for 30 min. After blocking, the cells were incubated first with primary antibodies (Table 2) overnight at 4°C, and then with Cy3-conjugated goat anti-rabbit IgG antibody (1:200; Sigma-Aldrich) and 5 μg/mL DAPI (Sigma-Aldrich) at room temperature for 30 min. Then, the cells were thoroughly washed with TBST and viewed through a fluorescence microscope (DMI3000; Leica).

Alkaline phosphatase staining

Alkaline phosphatase (AP) activity of human iPS cells, which were cultured on MEFs, was determined using the AP substrate kit (Sigma-Aldrich) according to the manufacturer's instructions [28].

Flow cytometric analysis of DNA content by PI staining

All steps were according to the previously described [29–32]. Briefly, each group cells was washed by PBS on three times, and fixed in 70% ice-cold ethanol, and kept in a freezer more than 48 h. Before flow cytometric analysis, the fixed cells were centrifuged, washed twice with PBS, and resuspended in PI staining solution (Sigma Chemicals) containing 25 μg/mL PI and 40 μg/mL RNase A (Sigma Chemicals) and 0.3% Tween-20 (Sigma-Aldrich). The cell suspension, which was hidden from light, was incubated for 20 min at 4 C and analyzed using the FACS (Quanta SC, Beckman Coulter). A total of 10,000 events were acquired for analysis, and the relative numbers of cell types, such as spermatid-like cells (1C = haploid), somatic cells, or iPS cells (2C = diploid) and primary spermatocyte-like cells (4C = tetraploid) were calculated using CellQuest software.

Teratoma formation

All animal procedures were carried out at Shanghai Tongji University with Institutional Animal Care and Use Committee approval in accordance with institutional guidelines. The 1×10^6 human iPS cells were inoculated into the hind leg of severe combined immunodeficient (SCID) mice. Teratomas were embedded in paraffin and histologically examined after hematoxylin and eosin staining. The procedure of teratoma formation experiment was performed as described [28].

Cell protein extraction, digestion, and labeling with iTRAQ reagents and data analysis

All steps of protein extraction and labeling were according to the previously described [34–43]. Protein identification and quantification for iTRAQ samples were carried out using ProteinPilot software (version 3.0; Applied Biosystems, MDS-Sciex). The search was performed against IPI human database (version 3.45). The search was performed using Paragon Algorithm, which is discussed in detail elsewhere. Only those proteins identified with at least 95% confidence were taken into account. All results were then exported into Excel for manual data interpretation [34–43].

Statistical analysis

Each experiment was performed as least three times, and data are shown as the mean ± SE where applicable, and differences were evaluated using Student's *t*-tests. The probability of < 0.05 was considered to be statistically significant.

Results

Analysis and identification of miR-122 and the 3′-UTR of TNP2 mRNA

The precursor miRNA sequences, mature miRNA sequences, chromosomal locations, and the length of miR-122 and the target gene *TNP2* were analyzed in several species using the online miRBase Target database (www.mirbase.org). Seven putative miRNA target sites were identified in the 3′-UTR of *TNP2* mRNA, which were conserved to varying degrees across species (Supplementary Fig. S2). For this study, we focused on human miR-122, which may target the human *TNP2* 3′-UTR (Supplementary Fig. S2). Luciferase reporter gene plasmids expressing the *TNP2* mRNA 3′-UTR [wild-type (wt) *TNP2*, empty plasmid, or

mutant *TNP2*] were co-transfected with miR-122 expression vectors (wt miR-122, empty vector, and mutant miR-122) into the mouse embryonic fibroblast cell line NIH-3T3, to examine whether mature miR-122-regulated expression of the *TNP2* gene. Luciferase activity of the wt *TNP2* 3′-UTR reporter gene was significantly inhibited by wt miR-122 (Supplementary Fig. S2), while the luciferase activity of the mutated *TNP2* 3′-UTR reporter gene was not inhibited by wt miR-122, indicating that miR-122 targets the *TNP2* 3′-UTR.

Pluripotency of iPS cells after differentiation into spermatozoa-like cells

We previously reported the successful generation of iPS cells from $CD34^+$ human amniotic fluid cells (HuAFCs) by transduction with lentiviral constructs encoding only *Oct4* [28]. In this study, we assayed the pluripotency of iPS cells. The AP activity of human iPS cells was very high, as represented by deep blue staining on the surface of the colonies (Fig. 1). In addition, immunofluorescence (IF) staining

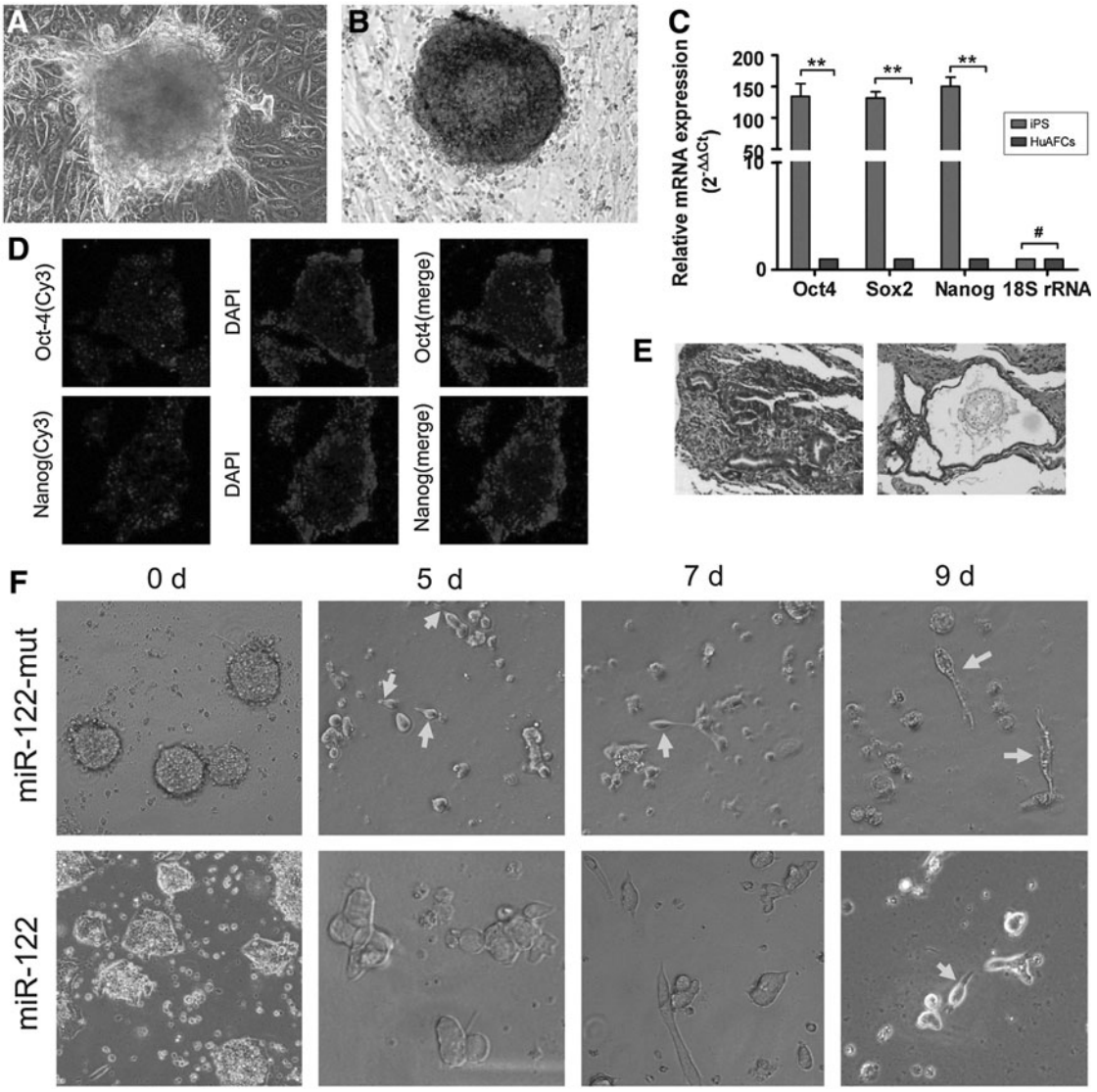

FIG. 1. Characterization of reprogrammed human induced pluripotent stem (iPS) cells differentiated into spermatozoa-like cells. **(A)** Characterization of reprogrammed human iPS cells. **(A)** Bright-field image of human iPS cells in the seventh phase of culture on HuAEC feeder layers. Original magnification, 200×. **(B)** Immunohistochemical staining for AP activity in a human iPS cell colony. AP activity in human iPS cells cultured on HuAECs was steady in the seventh phase. Original magnification, 200×. **(C)** Quantitative real-time PCR analysis of the transcription of endogenous stem cell markers (*Oct4, Nanog*, and *Sox2*) in human iPS cells in comparison with human amniotic fluid cells (HuAFCs); $^{**}P < 0.01$ versus HuAFCs; $^{\#}P > 0.05$ versus HuAFCs; $n = 3$. **(D)** Immunostaining of human iPS cells using anti-Nanog and anti-Oct4 antibodies. Original magnification, 200×. **(E)** Histology of teratomas in severe combined immunodeficient (SCID) mice and histology of a teratoma composed of ectodermal, endodermal, and mesodermal tissue. Original magnification, 100×. **(F)** On the ninth day after induction, the majority of iPS cells transfected with miR-122-mut exhibited human spermatozoa-like morphology, with a tapered head and long tail. However, this sperm-like morphology was not obvious in the miR-122-transfected group. Original magnification, 200×. HuAEC, human amnion epithelial cell.

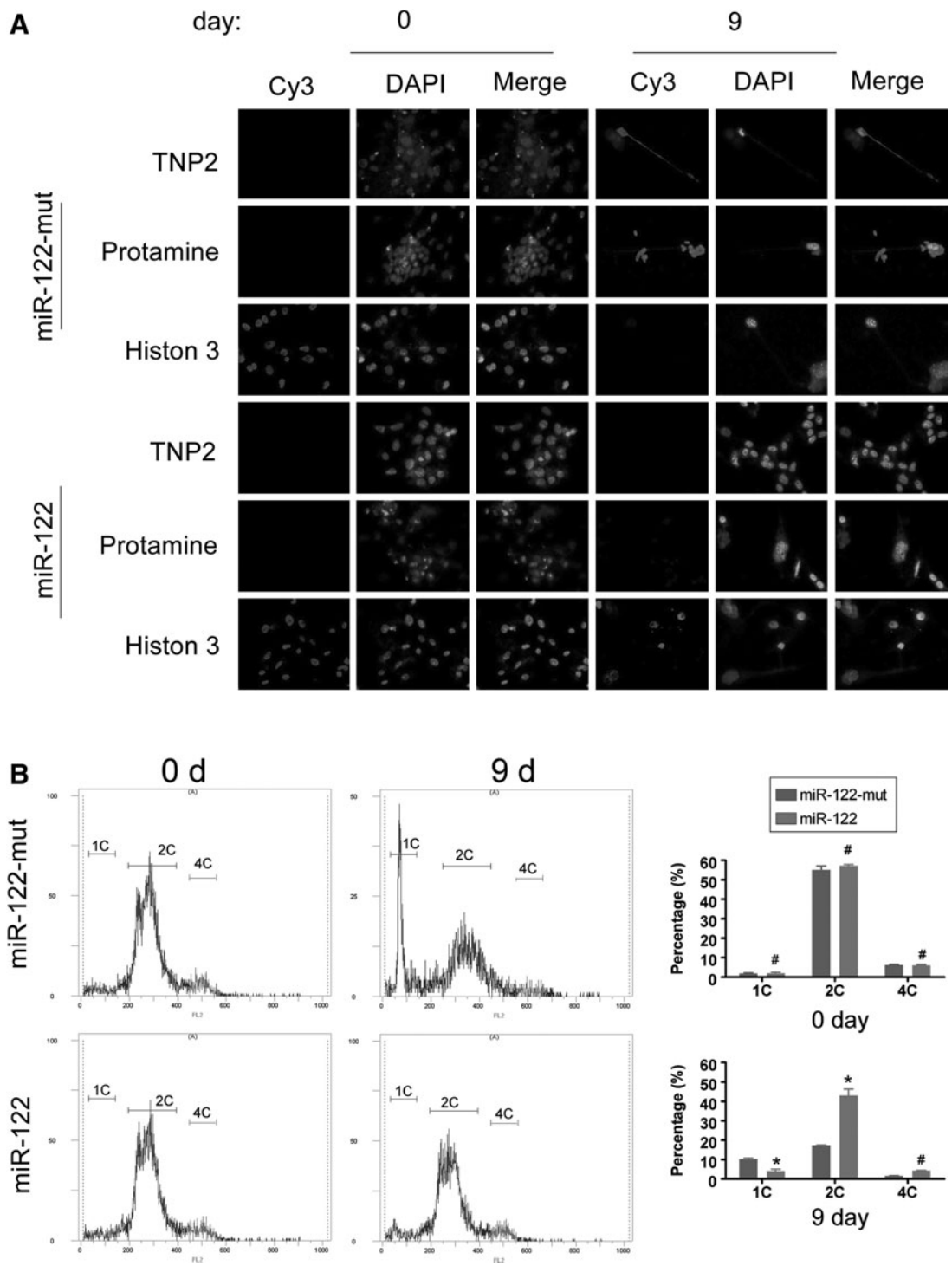

FIG. 2. Immunofluorescence (IF) analysis and flow cytometry analysis (FCA) of the haploid subpopulation in spermatozoa after induction. **(A)** IF staining was performed 9 days after induction to compare the expression levels of a somatic cell marker (histone 3) and male germ cell markers (protamine and TNP2) in miR-122-transfected and miR-122-mut-transfected iPS groups. Expression levels of protamine and TNP2 were higher in the miR-122-mut-transfected iPS group than in the miR-122-transfected iPS group. However, histone 3 levels in the miR-122-mut-transfected iPS group were lower than in the miR-122-transfected iPS group after differentiation. Original magnification, 200×. **(B)** On the ninth day after induction, FCA data clearly showed a typical 1C peak followed by a 2C peak and a 4C peak, indicating the presence of some haploid cells in the miR-122-mut-transfected iPS cells. However, although the IC peak was always present in the miR-122-transfected iPS cells, this population contained significantly fewer haploid cells than the miR-122-mut-transfected group. $^{*}P < 0.05$ versus miR-122-mut-transfected iPS cells; $^{\#}P > 0.05$ versus miR-122-mut-transfected iPS cells; $n = 3$.

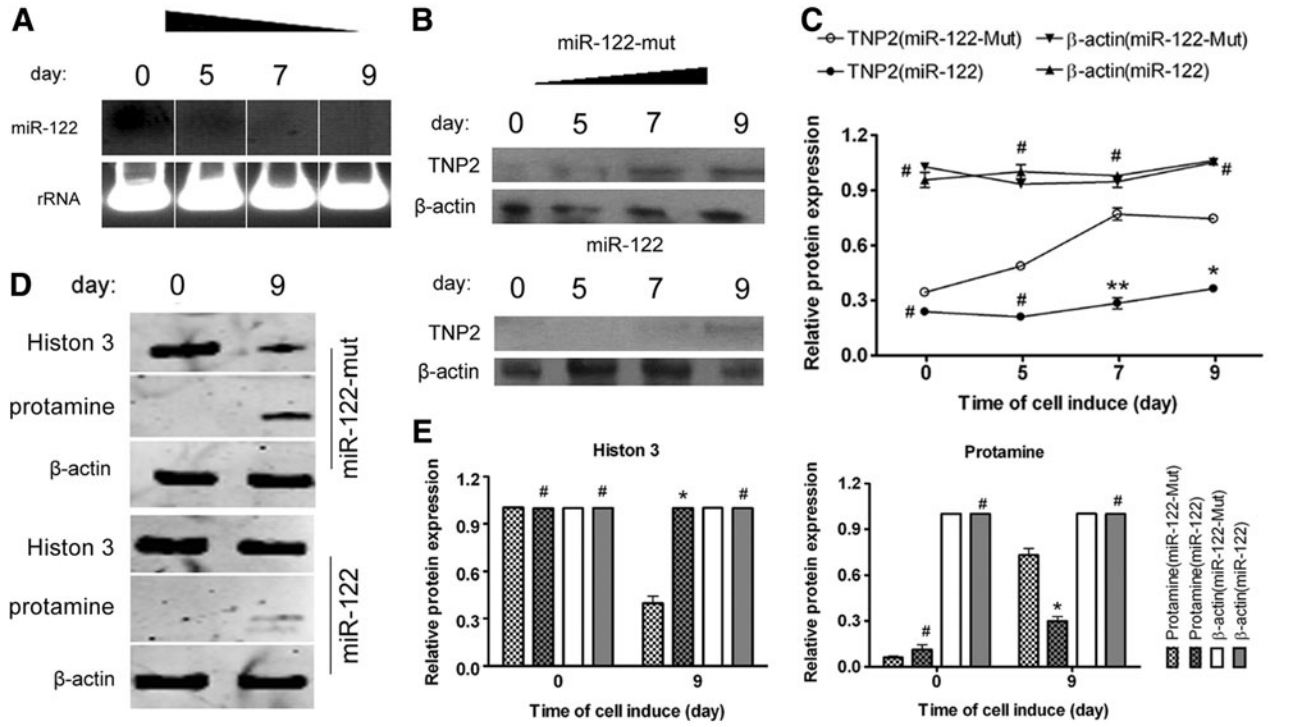

FIG. 3. miR-122 suppresses TNP2 expression to influence the transformation of iPS cells into spermatozoa-like cells. **(A)** When human iPS cells were induced to differentiate into spermatozoa-like cells in vitro, northern blotting revealed that the endogenous miR-122 hybridization signal gradually weakened with time. **(B, C)** Western blotting analysis carried out during induction showed that TNP2 protein was expressed at low levels in miR-122-transfected iPS cells, but not in miR-122-mut-transfected cells. After induction of the cells in vitro, TNP2 expression steadily increased over time in miR-122-mut-transfected iPS cells; $^{**}P<0.01$ versus miR-122-mut-transfected iPS cells; $^{*}P<0.05$ versus miR-122-mut-transfected iPS cells; $^{\#}P>0.05$ versus miR-122-mut-transfected iPS cells; $n=3$. **(D, E)** Furthermore, western blotting revealed that on the ninth day after induction, the levels of histone 3 were significantly higher in miR-122-transfected iPS cells than in miR-122-mut-transfected cells. In contrast, the expression of protamine was lower in miR-122-transfected iPS cells than in miR-122-mut-transfected cells. However, there were no significant differences in the expression levels of these proteins in both groups; $^{**}P<0.01$ versus miR-122-mut-transfected iPS cells; $^{*}P<0.05$ versus miR-122-mut-transfected iPS cells; $^{\#}P>0.05$ versus miR-122-mut-transfected iPS cells; $n=3$.

revealed that the expression levels of the pluripotent stem cell markers Nanog and Oct4 were increased in the iPS colonies (Fig. 1). Similar to the results of the IF staining, qRT-PCR analysis revealed that the expression levels of these stem cell markers were ~150-fold higher in human iPS cells than in HuAFCs (Fig. 1). In addition, in the in vivo xenograft experiments, SCID mice that were injected with iPS cells developed teratomas on the legs. Meanwhile, the iPS-derived teratomas contained cellular representatives of all three germ layers (Fig. 1). Based on these results, we concluded that the human iPS cells derived from HuAFCs possessed strong pluripotency.

In order to induce the in vitro differentiation of iPS cells into spermatozoa-like cells, the specific cell inducing factors were used. After defining the EB cell formation, miR-122-transfected and miR-122-mut-transfected cells were allowed to differentiate for 10 days. Five days after induction, bright-field microscopy revealed elongated unilateral projections on some miR-122-mut-transfected iPS cells. However, the miR-122-transfected cells did not show this morphology at 5 days after induction (Fig. 1). Over time, the number of cells with protrusions increased and the cell protrusions became more slender in the miR-122-mut-transfected group. At 9 days after induction, the majority of iPS cells transfected with miR-122-mut exhibited a similar morphology to human spermatozoa, with a tapering head and long tail. However, this morphology was not visible in the miR-122-transfected cells.

miR-122 reduces the ability of iPS cells to express spermatozoa markers during induction

First, we used immunofluorescent analysis of several markers of spermatozoa to determine whether the induced cells were spermatozoa-like cells. IF staining was performed 9 days after induction, to compare the expression levels of a somatic cells marker (histone 3) and male germ cell markers (PRM and TNP2) in both groups. The protein expression levels of PRM and TNP2 were elevated in the miR-122-mut-transfected iPS group, compared with the miR-122-transfected iPS group. However, after differentiation, the expression levels of histone 3 were lower in the miR-122-mut-transfected iPS cells than the miR-122-transfected iPS cells. Next, flow cytometry analysis (FCA) was used to analyze the DNA content and haploid subpopulation during the induction. On day 0, the DNA contents of the two groups showed no significant difference (Fig. 2), consisting largely of the 2C DNA population and a small population of 4C DNA cells. However, at day 9 after induction, FCA data clearly showed a typical 1C peak, followed by a 2C peak and a 4C peak in the

Table 3. iTRAQ Analysis of Differentially Expressed Proteins in Different Cell Groups

No.	*Accession*	*Gene symbol*	*Name*	*%Cov*	*Peptides (95%)*	*121:118*	P *value 121:118*
1	IPI:IPI00553177.1	*SERPINA1*	Isoform 1 of Alpha-1-antitrypsin precursor	82.06	24	12.35947037	9.37E-11
2	IPI:IPI00004573.2	*PIGR*	Polymeric immunoglobulin receptor precursor	64.14	6	6.546361923	0.000912243
3	IPI:IPI00023673.1	*LGALS3BP*	Galectin-3-binding protein precursor	89.06	20	4.285484791	5.02E-06
4	IPI:IPI00023014.1	*VWF*	von Willebrand factor precursor	47.49	19	2.779712915	4.37E-05
5	IPI:IPI00003590.2	*QSOX1*	Isoform 1 of Sulfhydryl oxidase 1 precursor	69.75	16	2.582259893	0.000261794
6	IPI:IPI00012269.3	*MMRN1*	Multimerin-1 precursor	57.25	11	1.887990952	0.001417065
7	IPI:IPI00021842.1	*APOE*	Apolipoprotein E precursor	95.90	23	0.501187205	0.001482379
8	IPI:IPI00783987.2	*C3*	Complement C3 precursor (Fragment)	81.48	62	0.478630096	2.47E-06
9	IPI:IPI00299503.2	*GPLD1*	Isoform 1 of Phosphatidylinositol-glycan-specific phospholipase D precursor	67.14	19	0.366437614	4.94E-06
10	IPI:IPI00022229.1	*APOB*	Apolipoprotein B-100 precursor	75.91	120	0.340408206	1.62E-09
11	IPI:IPI00292530.1	*ITIH1*	Inter-alpha-trypsin inhibitor heavy chain H1 precursor	79.03	34	0.220800504	0.000986809
12	IPI:IPI00339228.1	*FN1*	Isoform 8 of Fibronectin precursor	74.35	91	0.208929598	1.22E-09
13	IPI:IPI00410714.5	*HBA1/2*	Hemoglobin subunit alpha	71.83	10	0.203235701	0.006937179
14	IPI:IPI00305461.2	*ITIH2*	Inter-alpha-trypsin inhibitor heavy chain H2 precursor	72.62	32	0.177010894	2.65E-06
15	IPI:IPI00020996.3	*IGFALS*	IGFALS Insulin-like growth factor-binding protein complex acid labile chain precursor	65.62	12	0.124738403	2.22E-05
16	IPI:IPI00021841.1	*APOA1*	Apolipoprotein A-I precursor	97.38	23	0.114815399	1.17E-09
17	IPI:IPI00654755.3	*HBB*	Hemoglobin subunit beta	100	13	0.099083193	0.000101188

miR-122-transfected iPS cells, suggesting that miR-122-mut-transfected iPS cells contained ~10.2% of haploid cells (Table 3). However, although the 1C peak was consistently present in the miR-122-transfected iPS cells, these cells had a significantly lower population of haploid cells (4.08%) than the miR-122-mut-transfected group. These results suggest that reduced expression of miR-122 increased the ability of iPS cells to differentiate into spermatozoa-like cells.

miR-122 suppresses expression of TNP2 to influence the transformation of iPS cells into spermatozoa-like cells

Northern blotting revealed that the hybridization signal for endogenous miR-122 gradually weakened with time when human iPS cells were induced to differentiate into spermatozoa-like cells in vitro (Fig. 3). Thus, we speculated that miR-122 plays an important role in the differentiation of cells into spermatozoa. Furthermore, western blotting analysis showed that TNP2 was expressed at low levels in miR-122-transfected iPS cells during induction, but not in miR-122-mut-transfected cells (Fig. 3). After induction in vitro, the expression of TNP2 steadily increased over time in miR-122-mut-transfected iPS cells. The expression levels of histone 3 and PRM were determined by western blotting at days 0 and 9 after induction. On day 9 after induction, the levels of histone 3 in the miR-122-transfected iPS cells were significantly higher than the corresponding values in miR-122-mut-transfected cells. In contrast, the levels of PRM were lower in miR-122-transfected iPS cells than in miR-122-mut-transfected cells. However, there were no significant differences in the expression levels of these proteins in both groups (Fig. 3).

Relative and absolute quantification (iTRAQ) analysis and qRT-PCR to confirm differential protein expression in spermatozoa-like cells

The quantitative proteomics iTRAQ approach was employed to profile the differentially expressed proteins levels in the spermatozoa-like cells derived from iPS cells transfected with miR-122 or miR-122-mut. Spermatozoa-like cells from the miR-122-transfected iPS cells (SPC-miR-122) were used as the sample, and those from the miR-122-mut-transfected iPS cells (SPC-miR-mut) were used as the model. Proteins were considered upregulated and downregulated when their ratios were >1.5 and <0.5, respectively; these cutoffs are widely accepted and adopted. The samples were labeled with iTRAQ-121, and the model cells were labeled with iTRAQ-118. The iTRAQ ratio of 121:118 was used to identify the relative abundance of the protein. Additionally, to increase the coverage of protein identification and our confidence in the generated data, two separate preparations

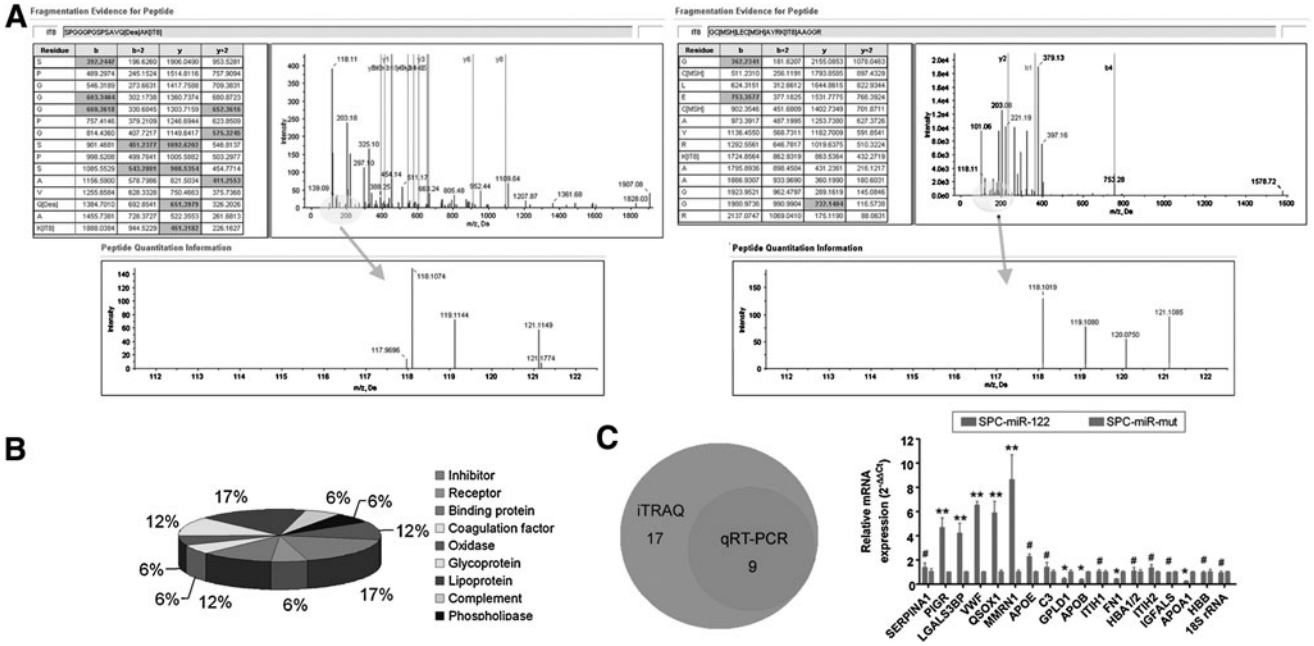

FIG. 4. The iTRAQ analysis of differentially expressed proteins in spermatozoa-like cells. **(A)** A representative MS/MS spectrum showing the peptides SPGGGPGSPSAVQ[Dea]AK[IT8] and GC[MSH]LEC[MSH]AYRK[IT8]AAGGR (*top panel*) from APOE and APOA1, respectively, with the representative quantitative information of the peptide (*bottom panel*). The ion assignments were as follows: miR-122-transfected iPS cells (SPC-miR-122), iTRAQ-121; miR-122-mut-transfected iPS cells (SPC-miR-mut) iTRAQ-118. **(B)** After filtering, the 17 differentially expressed proteins in the sample and model could be classified into 10 functional categories. **(C)** microRNA-specific quantitative real-time reverse transcription PCR (MiR-qRT-PCR) confirmed that five mRNAs (*PIGR, LGALS3BP, VWF*, *QSOX1*, and *MMRN1*), coding for the corresponding proteins identified by iTRAQ, were overexpressed in the SPC-miR-122 group compared to SPC-miR-mut group. Four of these mRNAs (*GPLD1, APOB, FN1*, and *APOA1*) were expressed at lower levels in SPC-miR-122 cells than SPC-miR-mut cells; $^{**}P < 0.01$ versus SPC-miR-mut; $^{*}P < 0.05$ versus SPC-miR-mut; $^{\#}P > 0.05$ versus SPC-miR-mut; $n = 3$.

were made, and each was analyzed by LC/MS/MS. A total of 780 unique proteins were identified with 95% confidence by the ProteinPilot search algorithm against the IPI human protein database v3.49 (Fig. 4). After filtering, a total of 17 proteins were found to have different expression levels between the sample and model (Table 3). Six proteins were found to be significantly overexpressed in the sample group as compared to the model. Conversely, 11 proteins were expressed at significantly lower levels in the sample than in the model. Molecular function classification of the 17 proteins was achieved using the Panther Classification (www.pantherdb.org). The 17 differentially expressed proteins could be classified into 10 functional categories on the basis of the PANTHER classification system (www.pantherdb.org; Fig. 4). Next, qRT-PCR was used to confirm the results of the iTRAQ analysis. Of the seven proteins that were identified to be overexpressed by iTRAQ (SERPINA1, PIGR, LGALS3BP, VWF, QSOX1, MMRN1, and APOE), qRT-PCR confirmed that five of the corresponding mRNAs (*PIGR, LGALS3BP, VWF, QSOX1,* and *MMRN1*) were overexpressed in SPC-miR-122 cells compared to SPC-miR-mut cells. The iTRAQ analysis revealed that 10 proteins were expressed at lower levels in SPC-miR-122 cells (C3, GPLD1, APOB, ITIH1, FN1, HBA1/2, ITIH2, IGFALS, APOA1, and HBB), and qRT-PCR analysis confirmed that four of these mRNAs (*GPLD1*, *APOB, FN1*, and *APOA1*) were expressed at lower levels in SPC-miR-122 cells than in SPC-miR-mut cells (Fig. 4).

Discussion

Approximately 40%–60% of cases of male infertility have been reported to be due to asthenospermia and abnormal sperm [31]. However, the mechanisms leading to the development of asthenospermia and abnormal sperm are not yet fully understood. Spermatogenesis is a long and complex process that occurs in the seminiferous tubule of the testis [29], which is regulated by multiple interactions between developing germ cells and the surrounding environment [29]. Spermiogenesis is the final stage of spermatogenesis, during which spermatids mature into motile spermatozoa. During this process, the nucleosomal structure undergoes major changes to condense the genome [9–11,44]. At this stage, several testis-specific subtypes of histone are synthesized and replace their somatic counterparts during the premeiotic, meiotic, and postmeiotic stages of the differentiation of germ cells [9–11]. Therefore, developing a suitable in vitro model would be helpful for studying the development of spermatozoa and the formation of sperm abnormalities. Although human embryonic stem cells (hESCs) and mouse spermatogonial stem cells (mSSCs) have been proposed as useful models for the study of the development of spermatozoa, and several studies have reported that sperm-like cells can be derived from hESCs or mSSCs, these cells have some shortcomings. In the case of hESCs, there are ethical restrictions for their use, the cell numbers are

limited, and the culture conditions are complex. Since mSSCs are derived from mice, differences between these cells and human sperm are inevitable. Based on the results of previous studies, we developed an in vitro method and induced the direct differentiation of human iPS cells into adult-type spermatozoa-like cells in this study. Human iPS cells are highly similar to hESCs in terms of morphology, proliferation, gene expression, and the epigenetic status of pluripotency-specific genes. Moreover, the use of human iPS cells can overcome the ethical problems associated with the use of hESCs and reduce the possibility of immune rejection; thus, these cells have the potential to become an attractive source for cell therapy [27,28,45].

We started by investigating epigenetic modifications, and analyzed the differential expression of miRNAs, which may influence the occurrence of abnormalities in sperm. Microarray analysis was used to determine and compare the miRNA expression patterns in infertile sperm and normal sperm. Based on previous investigations [20–22], we chose miR-122 as the object of study, and attempted to identify its role in the maturation and development of spermatozoa. We found that human iPS cells miR-122 with miR-122 could be induced to differentiate into human spermatozoa-like cells more efficiently than mutant miR-122-transfected cells. Furthermore, miR-122-transfected iPS cells showed increased morphogenesis of spermatozoa-like cells as well as a significant reduction in the number of haploid cells, as compared to mutant miR-122-transfected cells. Further studies showed that the *TNP2* gene is one of the target genes of miR-122. The *TNP2* expression level was downregulated by overexpression of miR-122. In mammals, chromatin condensation of spermatozoa development is a double-step event [12,14]: testis-specific histones are transiently replaced by TNPs and then by PRMs. Thus, both TNPs and PRMs are signs of sperm formation. However, after overexpression of miR-122 in human iPS cells during the induction of spermatozoa-like cells, the expression levels of TNP2 and PRMs were obviously lower in the miR-122-transfected group than in the mutant miR-122-transfected group. The expression levels of histone 3 showed the opposite trend. These results revealed that overexpression of miR-122 suppressed the expression of *TNP2* and PRM, and influenced the development and maturation of sperm cells.

Furthermore, iTRAQ labeling was used to identify the inhibition of other proteins due to miR-122 overexpression during sperm development. Recently, iTRAQ has been adopted for high-efficacy and high-throughput proteomic analysis of a variety of biological samples [34–43] such as cancer tissues, cells, plants, microorganisms, and sperm. In our study, we combined an easily accessible extraction buffer and a heat-induced antigen retrieval technique to retrieve the proteins from spermatozoa-like cells derived from human iPS transfected with miR-122 or mutant miR-122, followed by high-throughput proteomic iTRAQ analysis to identify and quantify proteins that are differentially expressed between the two groups. Expression of lipoproteins such as APOE, APOB, and APOA1 were most significantly different among all of the proteins analyzed in this study. Some previous reports indicated that genetic variation in the signal peptide of the *ApoB* gene was a risk factor for the development of male infertility [46,47]. Furthermore, male mice heterozygous for a targeted mutation of the *ApoB* gene exhibited male infertility due to sperm dysplasia [46,47]. Therefore, when miR-122 was overexpressed in iPS cells, the expression levels of not only TNP2 and PRM, but also other important proteins associated with sperm development, such as APOB, were inhibited.

In conclusion, differential expression of miR-122 may influence the differentiation of human iPS cells into spermatozoa-like cells, by suppressing expression of the miR-122 target gene *TNP2* and inhibiting the expression of other important proteins associated with sperm development, such as lipoproteins. These findings reveal that miR-122 is an important factor associated with abnormal sperm development.

Acknowledgments

This work was supported by grant from Shanghai Committee Medical Science Foundation of China (no.10411967100) and National Natural Science Foundation of China (no. 81202811), and Shanghai Municipal Health Bureau Fund (no. 20124320) to Te Liu.

Author Disclosure Statement

No competing financial interests exist.

References

1. Miyagawa Y, H Nishimura, A Tsujimura, Y Matsuoka, K Matsumiya, A Okuyama, Y Nishimune and H Tanaka. (2005). Single-nucleotide polymorphisms and mutation analyses of the TNP1 and TNP2 genes of fertile and infertile human male populations. J Androl 26:779–786.
2. Zenzmaier C, R Gerth, M Gruschwitz, H Lindner, E Plas and P Berger. (2011). Decreased levels of genuine large free hCG alpha in men presenting with abnormal semen analysis. Reprod Biol Endocrinol 9:114.
3. Hu W, H Yang, J Sun, Q Zhang, J Yang, L Lu, J Zhang, Y Qin, Y Xia and X Wang. (2011). Polymorphisms in CYP1B1 modify the risk of idiopathic male infertility with abnormal semen quality. Clin Chim Acta 412:1778–1782.
4. Chatzimeletiou K, A Sioga, L Oikonomou, S Charalampidou, P Kantartzi, V Zournatzi, D Panidis, DG Goulis, I Papadimas and BC Tarlatzis. (2011). Semen analysis by electron and fluorescence microscopy in a case of partial hydatidiform mole reveals a high incidence of abnormal morphology, diploidy, and tetraploidy. Fertil Steril 95: 2430.e1.
5. Moretti E, C Castellini, E Mourvaki, S Capitani, M Geminiani, T Renieri and G Collodel. (2011) Distribution of alpha- and delta-tocopherols in seminal plasma and sperm fractions of men with normal and abnormal semen parameters. J Androl 32:232–239.
6. Kowalczuk CI, RD Saunders and HR Stapleton. (1983). Sperm count and sperm abnormality in male mice after exposure to 2.45 GHz microwave radiation. Mutat Res 122:155–161.
7. Tseden K, O Topaloglu, A Meinhardt, A Dev, I Adham, C Muller, S Wolf, D Bohm, G Schluter, W Engel and K Nayernia. (2007). Premature translation of transition protein 2 mRNA causes sperm abnormalities and male infertility. Mol Reprod Dev 74:273–279.
8. Shirley CR, S Hayashi, S Mounsey, R Yanagimachi and ML Meistrich. (2004). Abnormalities and reduced reproductive

potential of sperm from Tnp1- and Tnp2-null double mutant mice. Biol Reprod 71:1220–1229.
9. Liu TD, BY Yu, FH Luo, XL Zhang, SC Wu, LH Liu and YJ Wu. (2011). Gene expression profiling of rat testis development during the early post-natal stages. Reprod Domest Anim 47:724–731.
10. Aoki VW, GL Christensen, JF Atkins and DT Carrell. (2006). Identification of novel polymorphisms in the nuclear protein genes and their relationship with human sperm protamine deficiency and severe male infertility. Fertil Steril 86:1416–1422.
11. Pradeepa MM and MR Rao. (2007). Chromatin remodeling during mammalian spermatogenesis: role of testis specific histone variants and transition proteins. Soc Reprod Fertil Suppl 63:1–10.
12. Chioccarelli T, G Cacciola, L Altucci, SE Lewis, L Simon, G Ricci, C Ledent, R Meccariello, S Fasano, R Pierantoni and G Cobellis. (2010). Cannabinoid receptor 1 influences chromatin remodeling in mouse spermatids by affecting content of transition protein 2 mRNA and histone displacement. Endocrinology 151:5017–5029.
13. Bizzaro D, GC Manicardi, PG Bianchi, U Bianchi, E Mariethoz and D Sakkas. (1998). In-situ competition between protamine and fluorochromes for sperm DNA. Mol Hum Reprod 4:127–132.
14. Becker S, Y Soffer, LM Lewin, L Yogev, L Shochat and R Golan. (2008). Spermiogenesis defects in human: detection of transition proteins in semen from some infertile men. Andrologia 40:203–208.
15. Zhao M, CR Shirley, S Mounsey and ML Meistrich. (2004). Nucleoprotein transitions during spermiogenesis in mice with transition nuclear protein Tnp1 and Tnp2 mutations. Biol Reprod 71:1016–1025.
16. Zhao XY, W Li, Z Lv, L Liu, M Tong, T Hai, J Hao, CL Guo, QW Ma, et al. (2009). iPS cells produce viable mice through tetraploid complementation. Nature 461:86–90.
17. Balhorn R. (2007). The protamine family of sperm nuclear proteins. Genome Biol 8:227.
18. Roque A, I Ponte and P Suau. (2011). Secondary structure of protamine in sperm nuclei: an infrared spectroscopy study. BMC Struct Biol 11:14.
19. Liu T, W Cheng, Y Gao, H Wang and Z Liu. (2012). Microarray analysis of microRNA expression patterns in the semen of infertile men with semen abnormalities. Mol Med Report 6:535–542.
20. Dai L, CH Tsai-Morris, H Sato, J Villar, JH Kang, J Zhang and ML Dufau. (2011). Testis-specific miRNA-469 up-regulated in gonadotropin-regulated testicular RNA helicase (GRTH/DDX25)-null mice silences transition protein 2 and protamine 2 messages at sites within coding region: implications of its role in germ cell development. J Biol Chem 286:44306–44318.
21. Yu Z, T Raabe and NB Hecht. (2005). MicroRNA Mirn122a reduces expression of the posttranscriptionally regulated germ cell transition protein 2 (Tnp2) messenger RNA (mRNA) by mRNA cleavage. Biol Reprod 73:427–433.
22. Yu Z and NB Hecht. (2008). The DNA/RNA-binding protein, translin, binds microRNA122a and increases its in vivo stability. J Androl 29:572–579.
23. Wu S, S Huang, J Ding, Y Zhao, L Liang, T Liu, R Zhan and X He. (2010). Multiple microRNAs modulate p21Cip1/Waf1 expression by directly targeting its 3′ untranslated region. Oncogene 29:2302–2308.
24. Cheng W, T Liu, F Jiang, C Liu, X Zhao, Y Gao, H Wang and Z Liu. (2011). microRNA-155 regulates angiotensin II type 1 receptor expression in umbilical vein endothelial cells from severely pre-eclamptic pregnant women. Int J Mol Med 27:393–399.
25. Zhang L, T Liu, Y Huang and J Liu. (2011). microRNA-182 inhibits the proliferation and invasion of human lung adenocarcinoma cells through its effect on human cortical actin-associated protein. Int J Mol Med 28:381–388.
26. Cheng W, T Liu, X Wan, Y Gao and H Wang. (2012). MicroRNA-199a targets CD44 to suppress the tumorigenicity and multidrug resistance of ovarian cancer-initiating cells. FEBS J 279:2047–2059.
27. Liu T, W Cheng, Y Huang, Q Huang, L Jiang and L Guo. (2011). Human amniotic epithelial cell feeder layers maintain human iPS cell pluripotency via inhibited endogenous microRNA-145 and increased Sox2 expression. Exp Cell Res 318:424–434.
28. Liu T, G Zou, Y Gao, X Zhao, H Wang, Q Huang, L Jiang, L Guo and W Cheng. (2012). High efficiency of reprogramming CD34(+) cells derived from human amniotic fluid into induced pluripotent stem cells with Oct4. Stem Cells Dev 21:2322–2332.
29. Lee JH, HJ Kim, H Kim, SJ Lee and MC Gye. (2006). In vitro spermatogenesis by three-dimensional culture of rat testicular cells in collagen gel matrix. Biomaterials 27:2845–2853.
30. Hayashi K, H Ohta, K Kurimoto, S Aramaki and M Saitou. (2011). Reconstitution of the mouse germ cell specification pathway in culture by pluripotent stem cells. Cell 146:519–532.
31. Easley CAt, BT Phillips, MM McGuire, JM Barringer, H Valli, BP Hermann, CR Simerly, A Rajkovic, T Miki, KE Orwig and GP Schatten. (2012). Direct differentiation of human pluripotent stem cells into haploid spermatogenic cells. Cell Rep 2:440–446.
32. Yu Z, P Ji, J Cao, S Zhu, Y Li, L Zheng, X Chen and L Feng. (2009). Dazl promotes germ cell differentiation from embryonic stem cells. J Mol Cell Biol 1:93–103.
33. Liu T, Q Chen, Y Huang, Q Huang, L Jiang and L Guo. (2012). Low microRNA-199a expression in human amniotic epithelial cell feeder layers maintains human-induced pluripotent stem cell pluripotency via increased leukemia inhibitory factor expression. Acta Biochim Biophys Sin (Shanghai) 44:197–206.
34. Gan CS, PK Chong, TK Pham and PC Wright. (2007). Technical, experimental, and biological variations in isobaric tags for relative and absolute quantitation (iTRAQ). J Proteome Res 6:821–827.
35. Chong PK, H Lee, J Zhou, SC Liu, MC Loh, TT Wang, SP Chan, DT Smoot, H Ashktorab, et al. (2010). ITIH3 is a potential biomarker for early detection of gastric cancer. J Proteome Res 9:3671–3679.
36. Chong PK, CS Gan, TK Pham and PC Wright. (2006). Isobaric tags for relative and absolute quantitation (iTRAQ) reproducibility: Implication of multiple injections. J Proteome Res 5:1232–1240.
37. Pham TK, P Sierocinski, J van der Oost and PC Wright. (2010). Quantitative proteomic analysis of Sulfolobus solfataricus membrane proteins. J Proteome Res 9:1165–1172.
38. Han CL, CW Chien, WC Chen, YR Chen, CP Wu, H Li and YJ Chen. (2008). A multiplexed quantitative strategy for membrane proteomics: opportunities for mining therapeutic targets for autosomal dominant polycystic kidney disease. Mol Cell Proteomics 7:1983–1997.

39. Ye H, L Sun, X Huang, P Zhang and X Zhao. (2010). A proteomic approach for plasma biomarker discovery with 8-plex iTRAQ labeling and SCX-LC-MS/MS. Mol Cell Biochem 343:91–99.
40. Xiao Z, G Li, Y Chen, M Li, F Peng, C Li, F Li, Y Yu, Y Ouyang and Z Chen. (2010). Quantitative proteomic analysis of formalin-fixed and paraffin-embedded nasopharyngeal carcinoma using iTRAQ labeling, two-dimensional liquid chromatography, and tandem mass spectrometry. J Histochem Cytochem 58:517–527.
41. Dean RA and CM Overall. (2007). Proteomics discovery of metalloproteinase substrates in the cellular context by iTRAQ labeling reveals a diverse MMP-2 substrate degradome. Mol Cell Proteomics 6:611–623.
42. Datta A, JE Park, X Li, H Zhang, ZS Ho, K Heese, SK Lim, JP Tam and SK Sze. (2010). Phenotyping of an in vitro model of ischemic penumbra by iTRAQ-based shotgun quantitative proteomics. J Proteome Res 9:472–484.
43. Bantscheff M, M Boesche, D Eberhard, T Matthieson, G Sweetman and B Kuster. (2008). Robust and sensitive iTRAQ quantification on an LTQ Orbitrap mass spectrometer. Mol Cell Proteomics 7:1702–1713.
44. Khattri A, SS Bhushan, V Sireesha, NJ Gupta, BN Chakravarty, M Deendayal, S Prasad, L Singh and K Thangaraj. (2011). The TNP1 haplotype—GCG is associated with azoospermia. Int J Androl 34:173–182.
45. Liu T, Y Huang, L Guo, W Cheng and G Zou. (2012). CD44+/CD105+ human amniotic fluid mesenchymal stem cells survive and proliferate in the ovary long-term in a mouse model of chemotherapy-induced premature ovarian failure. Int J Med Sci 9:592–602.
46. Huang LS, E Voyiaziakis, DF Markenson, KA Sokol, T Hayek and JL Breslow. (1995). apo B gene knockout in mice results in embryonic lethality in homozygotes and neural tube defects, male infertility, and reduced HDL cholesterol ester and apo A-I transport rates in heterozygotes. J Clin Invest 96:2152–2161.
47. Peterlin B, B Zorn, M Volk and T Kunej. (2006). Association between the apolipoprotein B signal peptide gene insertion/deletion polymorphism and male infertility. Mol Hum Reprod 12:777–779.

Address correspondence to:
Dr. Te Liu
Shanghai Geriatric Institute of Chinese Medicine
Longhua Hospital
Shanghai University of Traditional Chinese Medicine
Shanghai 200031
China

E-mail: liute79@yahoo.com

Dr. Weiwei Cheng
International Peace Maternity and Child Health Hospital
Shanghai Jiaotong University
Shanghai 200030
China

E-mail: wwcheng29@163.com

Prof. Lihe Guo
Institute of Biochemistry and Cell Biology
Shanghai Institute for Biological Sciences
Chinese Academy of Sciences
Shanghai 200031
China

E-mail: guolihe@cell-star.com.cn

Received for publication November 22, 2012
Accepted after revision January 17, 2013
Prepublished on Liebert Instant Online January 17, 2013